RSC Publishing Faraday Discussions

FD175:In vitro Study of the Interaction of Heregulin Functionalized Magnetic-Optical Nanorods with MCF7 and MDA-MB-231 Cells

Journal:	*Faraday Discussions*
Manuscript ID:	FD-ART-05-2014-000115.R1
Article Type:	Paper
Date Submitted by the Author:	17-Jul-2014

Complete List of Authors:	Lesniak, Anna; University College Dublin, Kilinc, Devrim; University College Dublin, Rashdan, Suad; university of bahrain, physics Kriegsheim, Alex; University College Dublin, Ashall, Brian; University College Dublin, Physics Zerulla, Dominic; University College Dublin, Physics Kolch, Walter; UCD, Systems Biology Ireland Lee, Gil; Purdue University, School of Chemical Engineering

In Vitro Study of the Interaction of Heregulin Functionalized Magnetic-Optical Nanorods with MCF7 and MDA-MB-231 Cells

A. Lesniak[a†], D. Kilinc[a,†], Suad A. Rashdan[a,b] , A. von Kriegsheim[c], B. Ashall[d], D. Zerulla[d], W. Kolch[c], and G. U Lee[a,*]

DOI: 10.1039/b000000x [DO NOT ALTER/DELETE THIS TEXT]

Multifunctional nanoparticles that actively target specific cells are promising tools for cancer diagnosis and therapy. In this article we review the synthesis and surface chemistry of Fe-Au nanorods and their characterization using microscopy. The diameter of the rods used in this study was selected to be 150-200 nm so they did not enter the cells. The 80 nm long Au tips of the nanorods were functionalized with heregulin (HRG), and the micron-long Fe portion was coated with a polyethylene glycol monolayer to minimize non-specific interactions. Nanorods functionalized with HRG were found to preferentially bind to MCF7 cells that express high levels of the receptor tyrosine-protein kinase ErbB2/3. Magnetic tweezers measurements were used to characterize the kinetic properties of the bond between the HRG on the rods and ErbB2/3 on the surface of the cells.. The strong magnetization of Fe-Au nanorods makes them excellent candidates for *in vitro* and *in vivo* imaging, and magnetic therapeutic applications targeting cancer cells in circulation.

A. Introduction

Our capacity to synthesize nanoparticles of specific shape and composition has rapidly advanced over the last decade due to the significant interest that nanotechnology has received. It is now possible to design and synthesize multi-segmented and multi-layered nanoparticles of defined composition from two or more inorganic, organic, or biological materials.[1, 2] Novel nanoparticles have been developed for biomedical and biotechnological applications where they play an important role in *in vitro* diagnostics, *in vivo* imaging, vaccines, and therapeutics, due to their strong interaction with electromagnetic fields and ability to interact with cells and biomolecules.[3] Of particular interest are multifunctional nanoparticles that act as highly sensitive contrast agents for cancer diagnosis as well as carriers of small molecule or biomolecular therapeutic agents. For example, gold nanoparticles can be readily functionalized with antibodies and polynucleotides, and act as contrast agents for X-ray based computer tomography and near infrared imaging when excited at their plasmon resonance frequencies. Even more interestingly, coating Au nanoparticles on dielectric spheres has been found to enhance their optical properties.[4] Superparamagnetic iron oxide nanoparticles (SPIONs) have also been used for targeting and imaging of specific cancers *in vivo* [3] and the fact that these nanomaterials also adsorb magnetic radiation has led to their use as agents for hypothermia therapy.[5, 6]

Targeting of specific cell types *in vivo* for diagnostic and therapeutic purposes has remained a challenge due to the numerous macromolecular components of blood that adsorb on nanoparticles and the body's multiple mechanisms for clearing nanoparticles from the circulation.[7, 8] Nanoparticle surfaces are typically coated with a polymer monolayer, such as, dextran or polyethyleneglycol (PEG), to improve their stability and biocompatibility, and prolong their blood half-life. These polymer coatings decrease the amount of protein that adsorb on the nanoparticle surface and increase the hydrodynamic size of the particles sparing the smaller particles from rapid elimination in the reticuloendothelial system. To target specific cell types, nanoparticles need to be further functionalized with agents that recognize specific molecules presented on the target tissues. Nanoparticles have been synthesised that are capable of targeting a variety of proteins that are over-expressed on certain types of solid tumours, i.e., folate receptors via folic acid,[9] integrin $\alpha_v\beta_3$ via RGD peptide,[10] and mutant epidermal growth factor (EGF) receptor EGFRvIII via a specific antibody.[11] Unfortunately, these receptors are rarely unique to cancerous tissues and this leads to the targeting of the nanoparticle to additional regions in the body. Studies of the interaction of nanoparticles with cultured cell lines indicate that they also non-specifically interact with cells that have poorly regulated endocytic pathways. For example, the enhanced permeability and retention effect (EPR) has been used to target cancers with nanoparticles based on particle size.[12-14] Ideally, nanoparticles' interaction with culture cells *in vitro* could be rapidly screened to determine the mechanism of particle-cell interaction before testing in animal models.

In this article we present the results of a study of the interaction of Fe-Au nanorods ~150-200 nm in diameter composed of segments of defined length with cultured cells using an optical microscope capable of tracking individual rods. The Fe-Au nanorods were functionalized with a PEG monolayer and heregulin (HRG), which is known to bind to a set of receptors that are over expressed in some breast cancers, i.e., the ErbB2/3 receptors. A novel microfluidics device is described that allowed the dynamics of the nanoparticle interactions with the cells to be studied in very small volumes under defined flow conditions in conjunction with magnetic tweezers measurements. This technique has been used to characterize the HRG functionalized nanorods' (NR-HRG) interaction with specific regions of two cell lines with known levels of expression of ErbB2/3. Magnetic tweezers has been used to characterize the interaction of the nanorods with the cells, which took place at the cell membrane since the particles appear not to be internalized. We suggest that these tools provide a powerful means to characterize nanoparticle-cell interactions *in vitro*, and the strong MRI contrast of the nanorods suggests that these studies can be translated to *in vivo* animal studies. B. Methods

B. Synthesis of Fe-Au two segmental nanorods

The PAA templates were synthesized by a three-step anodization method described previously.[14] A high-purity (99.999%)

piece of aluminium was electropolished in a mixture of 5 vol% sulphuric acid, 95 vol% phosphoric acid, and 20 g/L chromium oxide at 20 V and 60°C for 45 sec. This polished piece of aluminium was anodized in 0.42 M oxalic acid at 40 V and 0.9°C for 11 hours. The alumina layer was removed from the sample using an aqueous mixture of chromium oxide, phosphoric acid, and water (45 g/L / 3.5 vol% / 96.5 vol%) at room temperature for at least 5 hours. A second 6-hour anodization and 5-hour stripping step was conducted under the same conditions as described above. A third 5-hour anodization step produced highly ordered PAA template. The PAA was removed by immersing in saturated mercury chloride aqueous solution for 4 hours. The as-prepared PAA membrane was then immersed in phosphoric acid solution for pore widening for 10 min resulting in a pore diameter of approximately 60 nm.

The synthesis of segmented metal nanorods was based on the method developed described previously.[14] Briefly, an Au layer (ca. 200 nm) was sputtered on one side of the PAA template to serve as a working electrode in an electrochemical setup. An Ag/AgCl reference electrode and a Pt wire counter electrode was utilized to form a three-electrode configuration. The electrodeposition was controlled with a potentiostat/galvanostat. An Ag layer (ca. 2 µm) was first electrodeposited into the nanopores from a silver plating solution at a constant potential of -0.8 V (vs. Ag/AgCl). The Au and Fe layers were deposited from a commercial electroplating solution and freshly made iron sulphate solution ($FeSO_4$.7H2O, 120 g/L; boric acid, 45 g/L; ascorbic acid, 1 g/L), respectively, at -0.9 V (vs Ag/AgCl). The segmental length of each element was controlled by monitoring the charge during deposition, and 100 nm segments of Au and Fe required 0.003 and 0.009 Coulombs, respectively. The PAA membrane and Ag segment were removed with sodium hydroxide aqueous solution and fuming nitric acid, respectively. Dispersed Fe-Au nanorods were obtained after surface modification as follows: The nanorods were washed thoroughly with sodium hydroxide solution, deionised water, and ethanol. In a subset of experiments, Fe-Au rods 203.4±6.1 nm in diameter were synthesized using a commercial Al_2O_3 membrane filters with pore back-side diameters of ~200 nm as described above using following parameters: 125 mC for Au and 3C for Fe segments. Figure 1A presents scanning electron micrographs of the rods in which the gold sections can be easily identified due to higher propensity to scatter electrons.

Figure 1. A. Scanning electron micrographs showing synthesized Fe-Au nanorods with highly uniform size and element ratio. Scale bar = 1 µm. **B.** Cartoon depicting surface modifications: Fe segment is coated with PEG–methoxy (2); Au segment is coated with PEG–carboxyl (3) and conjugated with streptavidin (4). Free HRG was modified with biotin (5). Biotinylated HRG was bound to STR at the gold tips (6).

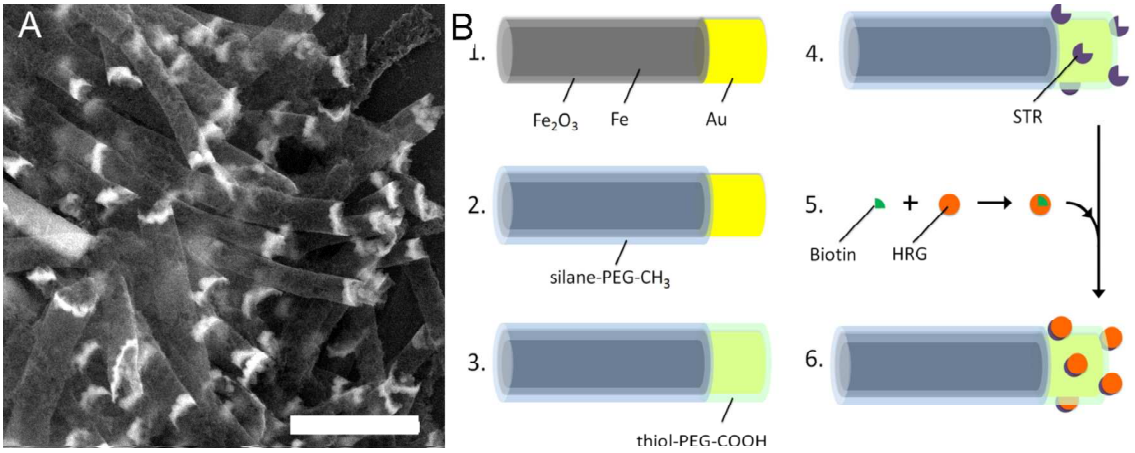

Surface chemistries

Fe-Au nanorods 203.4±6.1 nm in diameter, composed of 77.9±5.4 nm long Au and 1.35±0.07 µm long Fe segments, were coated with self-assembling PEG monolayers (Fig. 1B). First, the Fe segment was coated with methoxy-PEG via silane chemistry; then, the Au segment was coated with carboxyl-PEG via thiol chemistry. The Fe segment was coated with 1mg/mL methoxy-PEG-silane (2 kDa; Creative PEGWorks) dissolved in 2:1 mixture of toluene and triethylamine (Et3N). Following the overnight reaction at RT, pentane was added to precipitate the nanorods and the mixture was centrifuged. The precipitation step was repeated 3×. The Au segment was then coated with COOH-PEG-SH (3.4 kDa; Creative PEGWorks) dissolved in EtOH (1 mg/mL). Following the overnight reaction at RT, the nanorods were rinsed 3× with EtOH. Nanorods were dispersed in 2-(N-morpholino)ethanesulfonic acid (MES) buffer and incubated with a mixture of 1-ethyl-3-[3-dimethylaminopropyl]carbodiimide hydrochloride (EDC; Thermo Scientific) and N-hydroxysulfosuccinimide (Sulfo-NHS; Thermo) for 30 min, both 10 g/L, dissolved in MES buffer. After 3× PBS rinsing, particles were incubated with 0.6 g/L streptavidin (STR) in PBS for 2 hours at RT and overnight at 4°C. STR-conjugated nanorods (NR-STR) were rinsed 3× with and dispersed in PBS containing 0.02% Tween20. Recombinant HRG (R&D Systems) was biotinylated using sulfo-NHS-biotin at 20-fold excess of the latter. Excess biotin was removed using a spin column (Thermo). Biotinylated HRG (5 µM) was mixed with NR-STR in a rotating wheel for 1 hour, after which the nanorods were thoroughly rinsed with PBS.

Lab-on-a-chip and magnetic tweezers experiments

In vitro cell targeting experiments were conducted on cells cultured in a novel microfluidic device.[15] Polydimethylsiloxane (PDMS) microfluidic devices that have 4 mm long, 750 µm wide, and 75 µm high grooves were fabricated using photolithography and replica molding processes. Inlet and outlet holes were punched out of the PDMS and the devices were

permanently bonded to glass coverslips using oxygen plasma. MCF7 and MDA-MB-231 cells were seeded in UV-sterilized microfluidic devices at low confluence. Cells were starved prior to experiment by replacing full DMEM with serum free medium at least for 1 hour. The inlet and outlet wells of the channel were filled with 20 µl fresh medium, representative group of cells were located and imaging was started. Set volumes of HRG or STR-conjugated nanorod suspensions (10 µL) were added to the channels and flowed over the cells until the volume difference in the inlet and outlet reservoirs diminished. Imaging was conducted at 1 fps. Nanorods with a velocity lower than 15 µm/s and with a trajectory that traverses the cell area were considered for cell targeting analysis. For HRG competition experiments, MCF7 cells in microfluidic devices were incubated with medium containing soluble HRG at varying concentrations for 15 minutes. HRG-conjugated rods suspended in the same medium were introduced and cell targeting was quantified as described.

A custom-built electromagnet was used to apply forces on HRG-conjugated particles bound to MCF7 cells. Forces acting on the nanorods were calibrated by measuring their drag velocity in fluids of defined viscosity.[16] The force is a function of the distance between the tip of the electromagnet core and the nanorod, as well as the current passing through the coil. The magnitude of the applied force for given horizontal and vertical distance from the tip and for a given current was calculated through interpolation. Acting force per nanorod in each experiment was estimated by interpolating the force values measured at known distances and currents. The multilayer design of the microfluidics chips allows us to maintain an electromagnet tip–nanorod distance no more than 500 µm, which is critical for maximizing force in the cell stretching experiments. MCF7 cells cultured in these modified devices were targeted with HRG-conjugated nanorods as described. Live cell imaging was conducted at 1.5 fps while applying periodic stretch (1 s on, 1 s off) at different force magnitudes for 15 min.

C. Results and Discussion

Optical and magnetic properties of the nanorods

We have recently characterized the optical signature of the Fe-Au nanorods using transmission polarization microscopy.[14] Nanorods of length ~2 µm (~1 µm Fe and ~1 µm Au) and ~300 nm in diameter could be visualized in both bright field microscopy (Fig. 2A) and (Fig. 2B) crossed polarized optical microscopy, where the latter was achieved by using an orthogonally-aligned polarizer/analyzer pair. Sequential images in Figure 2B show how the scattered light intensity depends on the orientation of the rod where θ is the angle between the polarization axis and the rod's longitudinal axis. The optical signature of the gold nanorod was characterized by the polarization dependent change in the scattering intensity of the two bright stripes, which is a result of optical effects associated with the cylindrical geometry of the nanorod, the plasmonic modes excited on the Au section of the nanorod, the ultra-high collection angle of the 1.49 NA objective lens, and the illumination geometry. The dark stripe along the middle of the rod's longitudinal axis resulted from the shadow produced by the cylindrical rod when imaged in transmission direction. In contrast, light scattered from plasmonic modes, which have an altered polarization direction and scattered diffusely from the edges of the rod, can be detected by the wide-angle collection of the objective lens and pass through the analyzer.

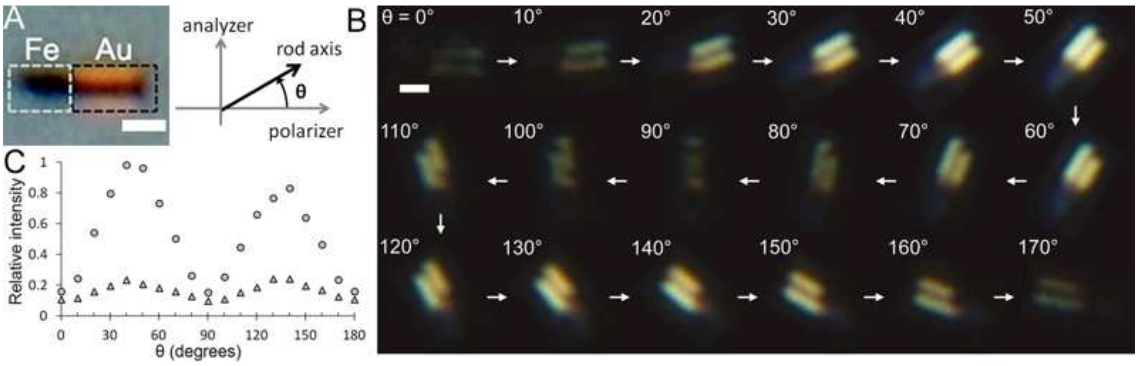

Figure 2. Optical signature of iron-gold composite nanorods. ***A.*** Bright-field image of a 295 nm diameter nanorod. ***B.*** A series of crossed polarisation microscopy images of the same rod (right panel) analyser where θ represents the angle between the incident polarisation plane and the nanorods orientation. Scale bars = 500 nm. ***C.*** Scattered light intensity from small (triangles) and large (circles) rods changes as a function of the angle (θ) between the polarizer and the rod axis.

Figure 2C presents the intensity of the optical signature of the rods that was measured from the images in Figure 2B as a function of θ. The minimum intensity was observed when the illumination polarization was oriented parallel to the longitudinal and transverse axes, i.e., θ of 0°, 90°, 180°, or 270°, and the maximum intensity was observed when the illumination polarization was orientated halfway between the longitudinal and transverse axes, i.e., θ of 45°, 135°, 225°, or 315°. The plasmonic contribution to this behaviour can be understood by considering three exemplary orientations. First, when the polarization was aligned parallel to the longitudinal axis of the nanorod, i.e., θ of 0° or 180°, the longitudinal axis plasmon was excited at a maximum level. However, the scattering was polarized along the longitudinal axis and thus was almost completely rejected at the analyzer resulting in the observed intensity minimum. Second, when the polarization was aligned perpendicular to the longitudinal axis of the nanorod, i.e., θ of 90° or 270°, the transverse axis plasmon was excited. Analogous to the previous case, upon scattering, this light had a polarization orientation aligned in the transverse direction that was rejected by the analyzer resulting in the observed minimum. Third, consider now the case where the polarization

was aligned halfway between the longitudinal and transverse orientations of the nanorod. In these cases, both longitudinal and transverse axis plasmonic modes were partially excited. However, as the resulting scattered light maintained the polarization defined by the plasmonic modes, the polarization lies at an angle of 45° or 135° to the polarizer and analyzer. When this light was analyzed a relatively large portion of the light passed through the analyzer maximizing the observed intensity. The relative intensity of light transferred through the polarization microscope provides a powerful technique that enabled the orientation of sub-wavelength nanorods to be defined in the far-field without visualization of the Fe section of the rod.

The magnetic properties of the Fe-Au nanorods were characterized with a SQUID magnetometer (Quantum Design, MPMS XL 7T). The magnetization measurements were performed on the nanorod arrays in the PAA membrane with the magnetic field oriented parallel and perpendicular to the longitudinal axis of the rods. The hysteresis loops indicated that the nanorods were magnetically soft and had an easy axis that is oriented along their longitudinal direction. The longitudinal coercive magnetization (H_c), remanent magnetization (M_r), and saturation magnetization (M_s) of the iron section of the nanorods were 40, 14.7±0.7, and 1457.7±73 emu/cc, respectively. The transverse H_c, M_r, and M_s of the iron section were 40, 17.7±0.9, and 1600±80 emu/cc, respectively. The magnetic properties of the Fe nanorods indicates that their saturation magnetization was quite close to that of bulk Fe, which is 1750 emu/cc or 220 emu/g.[17] An important feature of the magnetic properties of the Fe segment of the nanorods was that they were magnetically soft, which allowed the nanorods to be repeatedly used for magnetic separation without acquiring a residual magnetic moment. The hardness of the Fe nanorods are expected to be defined by the size of the iron domains formed during the electrodeposition and size of nanorods.[18] The size dependence of the magnetisation has been characterized for different sized rods, i.e., diameters of 60 and 295 nm, by their squareness, i.e., the ratio between the remanent and saturation magnetization, M_r/M_s.[19] Smaller rods were have a higher level of squareness than the larger rods, but the relatively low magnitude of squarenesses of all our nanorods suggest that the Fe rods are composed of multi-domain particles. This has been confirmed by high-resolution electron microscopy as shown in Figure 1B. The strong magnetic susceptibility, soft magnetic behaviour, and relatively large size of the class I rods make them an ideal material for magnetic tweezers and diagnostic applications.

Magnetic nanoparticles developed for drug delivery or theranostic applications, such as FePt capsules [20] and Fe_2O_3 tubes,[21] may also be optimized for magnetic tweezers applications like those presented in this article. Other potential candidates are the soft composite materials with programmable shape changes: Stripes that twist or bend,[22] and tubes that collapse upon exposure to weak magnetic fields [23] can be further exploited for their use as magnetic tweezers probes.

Targeting of ErbB2/3 receptors in cancer cell lines and magnetic tweezers measurements

Figure 3A illustrates that streptavidin (STR) was successfully localized to the Au tips of the nanorods using fluorescently-labeled biotin. STR also bound to bare Au, but not to unmodified carboxyl groups on a PEG monolayer. Localization of STR to Au tips was further verified by biotinylated fluorescent DNA (Fig. 3B). When NR-STR were reacted with PEG-biotin surfaces, the Fe segments were free to follow the external magnetic field around the Au tips that acted as pivot points (Fig. 3C). These observations cumulatively suggested that the two-step surface chemistry successfully functionalized Fe-Au nanorods with specific ligands for active targeting; yet minimized non-specific interactions, which can lead to the premature clearance and mis-targeting of nanoparticles *in vivo*.

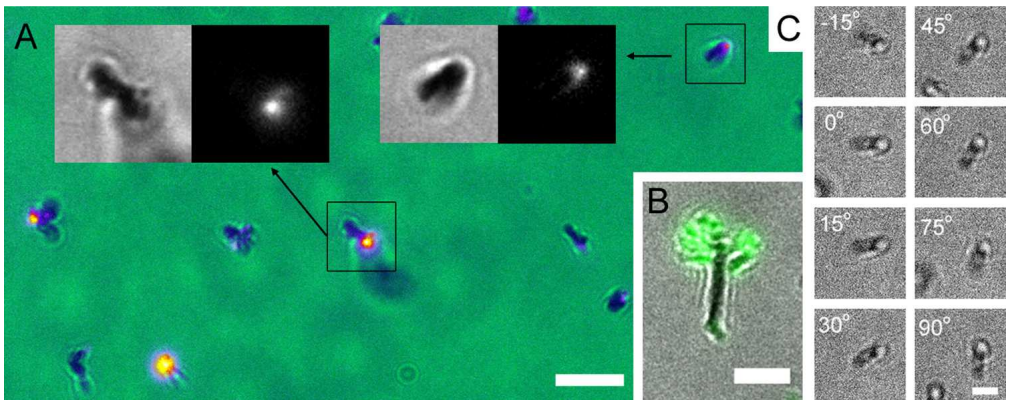

Figure 3. ***A.*** Streptavidin-conjugated nanorods (NR-STR) showing their fluorescent tips after incubation with fluorescein-biotin. Fluorescent image was pseudo-colored and superposed with the phase contrast image. Brightfield and fluorescent images of boxed areas are 2× magnified. ***B.*** NR-STR incubated with biotinylated fluorescein-DNA. ***C.*** NR-STR rotates freely around its gold tip attached to the PEG-biotin surface. Bars = 5μm (A) and 2μm (B, C).

ErbB2 and 3 receptors on two different human breast adenocarcinoma cell lines were targeted with NR-HRG. ErbB2 expression levels on both cell types were quantified by using immunofluorescence followed by fluorescence-activated cell sorting (FACS, data not shown) and ErbB3 expression was quantified through Western blotting (Fig. 4F). In agreement with previous studies,[24] ErbB3 expression was higher in MCF7 cells (Fig. 4F). When flown over cultured cells, NR-HRG successfully targeted MCF7 cells resulting in higher interaction rates compared to NR-HRG flown over MDA-MB-231 cells and NR-STR flown over MCF-7 cells (Fig. 4). Nanorod targeting rates for MCF7 relative to MDA-MB-231 cells correlated with their relative ErbB2 and 3 expression levels. Figures 4B and C present the paths of HRG-conjugated nanorods flowing over MCF7 and MDA cells, respectively, in microfluidic channels. HRG-conjugated rods that were reacted with the MCF7

cells exhibited significantly higher binding rates than those reacted with the MDA cells (Fig. 4E). There was also a significant level of interaction of STR-conjugated nanorods with MCF7 and MDA cells, which we attribute to nonspecific protein-protein interactions. A detailed microscopic analysis of particle targeting experiments revealed the non-uniform distribution of bound nanorods on cell surfaces. 'Active zones', dynamic extrusions in the cell periphery, attracted both HRG-conjugated rods, and to a lesser extent, STR-conjugated rods. HRG-conjugated rods targeted active zones six times more often than rest of the cell surface (30.7±7.9 vs. 4.9±0.8 rods per 1000 μm^2, $p < 0.005$), whereas STR-conjugated rods targeted active zones 3× more often than rest of the cell surface (18.8±4.5 vs. 6.3±0.8 rods per 1000 μm^2; $p < 0.01$). These results suggest that cells expressing specific surface receptors can be targeted with Fe-Au nanorods whose tips are functionalized with appropriate ligands.

Figure 4. A. Time-lapse images of MCF7 cells targeted with individual heregulin-conjugated Fe-Au nanorods (NR-HRG). Scale bar = 5 μm. Exemplary trajectories of permanently bound (green), interacting (yellow), and non-interacting (red) nanorods: NR-HRG on MDA-MB-231 (B) and MCF7 (C) cells, and streptavidin-conjugated nanorods on MCF7 cells (D). Scale bars = 5 μm. NR-HRG targeting rates (E) of MDA-MB-231 and MCF7 cells correlate with their ErbB3 expression levels shown by Western blots made using equal amount of MDA-MB-231 and MCF7 cells with antibodies against ErbB3 and GAPDH (F). Bars = 5μm. Boxed areas are 2.5× magnified.

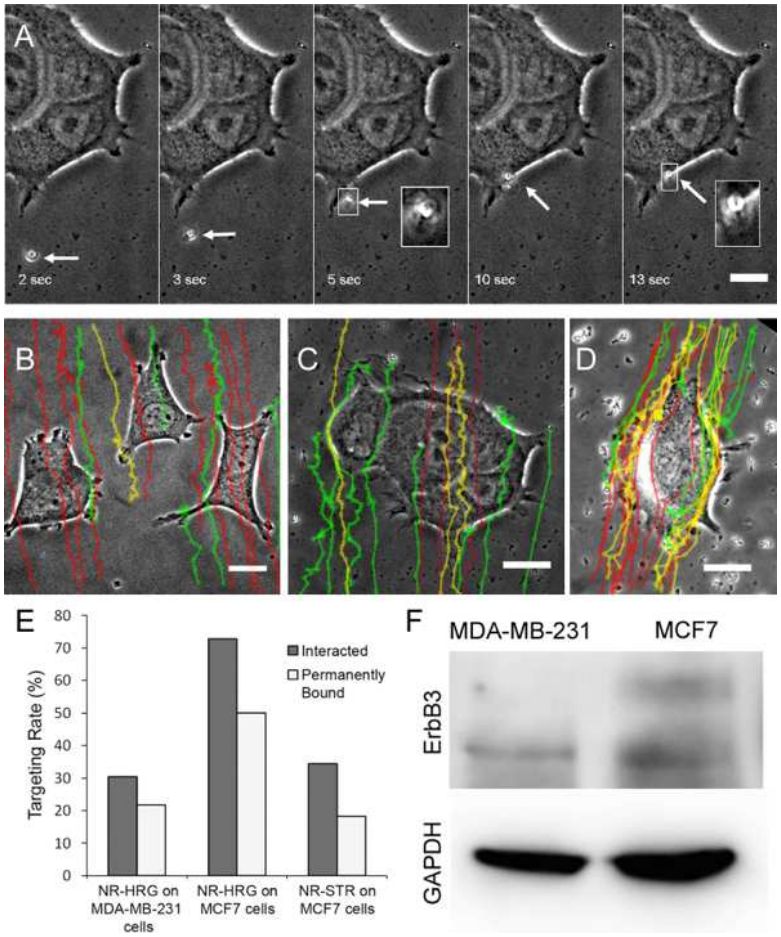

In order to determine whether targeting of HRG-conjugated nanorods was influenced by soluble HRG in binding to MCF7 cells, the in-flow cell targeting experiment was repeated by exposing the cells to increasing concentrations of soluble HRG. Particle binding rates were not affected by the presence of free HRG up to 100 nM, a concentration that is two orders of magnitude higher than that needed to induce prolonged activation of mitogen-activated protein kinase/extracellular signal-regulated kinase 1/2 (MAPK/ERK) pathway in these cells.[25] The local apparent concentration of HRG on the gold tips of rods was calculated by dividing the estimated number of HRG molecules to the contact volume, which is the contact area multiplied by the estimated diameter of the molecule. The number of molecules was estimated by adjusting the previously-measured surface coverage of a similarly sized heterobifunctional PEG coated on spherical particles.[16] The local apparent density was determined to be 300 μM, which may explain the lack of competition between HRG-nanorods and soluble HRG

in these experiments. Considering the (hetero) dimerization of ErbB2 and 3 receptors [26] and their relative HRG dissociation rates,[27] it appears that the very high local concentration of HRG at nanorod tips results in the formation of strong bonds with ErbB2/3 dimers.

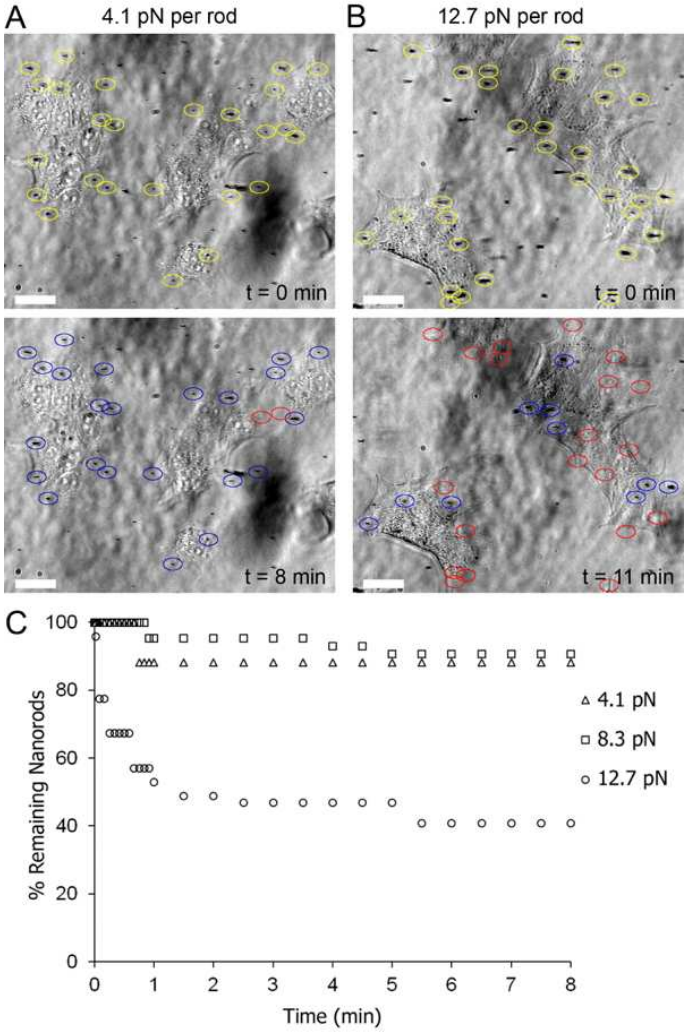

Figure 5. Exemplary snapshots of MCF7 cells targeted with NR-HRG which were mechanically stimulated by using a custom-built electromagnet. Yellow circles indicate bound nanorods immediately prior to force application (time = 0), and red and blue circles indicate escaped and remaining nanorods, respectively, at indicated time points. Scale bars = 20 µm. The plot shows the percentage of nanorods remaining on cell surface during periodic force application as a function of time. Only single nanorods were included in this analysis.

MCF7 cells specifically targeted with HRG-NR were mechanically stimulated by using a custom-built magnetic tweezers coupled to a modified microfluidic device that minimized the gap between the cells in the flow channel and the electromagnet core. Cyclic stretching forces at constant magnitude of 4.1, 8.3 and 12.7 pN were applied to cells targeted with individual rods over a fixed period of time. Receptor-ligand bonds withstand cyclic stretch at low force magnitudes but gradually failed at higher force magnitudes (Fig. 5). These results demonstrate that magnetic nanorods targeting specific membrane receptors form bonds that can withstand stretching forces. Due to the small size of the Au tips, the force will be distributed to a limited number of ErbB2/3 receptors.

The kinetic and energetic properties of protein-protein interactions can be analyzed through analysis of the magnetic tweezers results.[16, 28] The energy landscape of a chemical reaction may contain one or more sharp activation barriers that need to be overcome for the reaction to occur. External force application increases the unbinding rate by skewing this energy landscape.[29] According to Bell's model, the off-rate of a single, specific intermolecular interaction depends on the externally-applied constant force F

$$k_{off} = k_{off,o} \cdot \exp\left(F / f\right) \quad [1]$$

where $k_{off,0}$ is the dissociation rate of the interaction in the absence of an external force and f is the scaling force, characteristic of that interaction.[30] This model implies that weak, non-covalent bonds have a limited lifetime and will break under any level of force if pulled on for a sufficient time period. An extension of this model is proposed [31] for multiple parallel bonds of the same type where the off-rate also depends on the number of bonds, n

$$k_{off} = k_{off,o}\left(\sum_{i=1}^{n}\exp\left(\frac{(-x/(i\cdot f))}{i}\right)\right)^{-1} \quad [2]$$

In this study, constant magnetic forces were applied of 4, 8 and 13 pN at a frequency of 0.5 Hz to characterize the HRG-ErbB2/3 intermolecular bonds. Clearly, very few of the particles were displaced from the cells at the lower forces, but a significant number of particles were displaced at 13 pN of force. This behaviour is consistent with the formation of a small number of slip bonds between the nanorods and the cells.

D. Conclusions

Active cell targeting with multifunctional nanoparticles has recently gained considerable attention. Core-shell[32,33] and dumbbell-shaped[34] structures were proposed to obtain nanoparticles that contain both Au and Fe_3O_4. We have recently described the synthesis of Fe-Au nanorods that have high saturation magnetization, low remanence, uniform size and strong plasmonic activity.[14, 35] In this study, we targeted specific cancer cell receptors using large (Ø = 200 nm) magnetic nanorods with heregulin-functionalized Au tips. Nanorods functionalized with heregulin using a PEG monolayer selectively bound to the MCF7 target cells that have high levels of ErbB2/3 but did not enter the cells. These nanorods bind to cells displaying a low density of ErbB2/2 (i.e., MDA-MBA-231 cells) with a specificity similar to background levels as measured from the interaction of streptavidin-functionalized nanorods with MCF7 cells. Magnetic tweezers measurements indicate that the rods bind to the cells through a small number of receptors. This approach promises to allow us to develop a detailed understanding of the kinetics of interaction of nanoparticles with cell *in vitro*. More generally, the template synthetic approach employed here may also be scaled down to smaller (Ø < 50nm) nanorods, which are suitable for cell internalization *in vivo*. The anisotropic nature of Fe-Au nanorods also renders them potential agents for cell destruction therapy, where heating acting on internalized particles have been shown to induce apoptosis. The polycrystalline nature of the Fe segment makes these rods magnetically soft; yet their *Ms* is >10× higher than of SPIONs, which are widely used as MRI contrast agents.[36] Pure Fe NPs require >20× smaller concentration to generate the same amount of heat as SPIONs of similar size [37] and hence are more suitable for magnetic hyperthermia.[38] Due to these superior qualities, Fe-Au NRs also have the potential to replace SPIONs in targeted molecular imaging and/or hyperthermia, where high particle concentrations are needed.[38, 39] Thus, this study confirms that the physical and chemical properties of the nanorods can be tuned to selectively bind to cells expressing high level of receptors, and suggests that targeting metastasized cells in circulation for diagnostic applications could be highly selective.

Acknowledgments

We would like to acknowledge Manuel DaSilva, Timothy D. Sands, and Yong Zhang for their collaboration on the development of the Fe-Au nanorod synthesis techniques. This article is based on works supported by the Science Foundation Ireland under grants 08/RP1/B1376 (GUL), 08/IN1/B2072 (GUL), 06/CE/B1129 (AvK and WK), Erasmus Mundus Gulf Countries Postdoctoral Fellowship (SAR), and Marie Curie Intra-European Fellowship (DK). We thank the Conway Institute core facilities for providing the instrumentation.

References

a Conway Institute and School of Chemistry, UCD, Dublin, Ireland
b University of Bahrain, Kingdom of Bahrain
c Systems Biology Ireland, UCD Conway Institute, UCD, Dublin, Ireland
d School of Physics, UCD, Dublin, Ireland
† Equal contribution
* Corresponding author: Prof. Gil U. Lee, Bionanotechnology Group, University College Dublin, Belfield, Dublin 4, Ireland. Email: gil.lee@ucd.ie

1. J. Della Rocca, D. Liu and W. Lin, *Acc Chem Res*, 2011, **44**, 957-968.
2. M. A. Mahmoud, R. Narayanan and M. A. El-Sayed, *Acc Chem Res*, 2013, **46**, 1795-1805.
3. D. Yoo, J. H. Lee, T. H. Shin and J. Cheon, *Acc Chem Res*, 2011, **44**, 863-874.
4. S. Link and M. A. El-Sayed, *The Journal of Physical Chemistry B*, 1999, **103**, 4212-4217.
5. Q. A. Pankhurst, N. T. K. Thanh, S. K. Jones and J. Dobson, *Journal of Physics D: Applied Physics*, 2009, **42**, 224001.
6. K. Maier-Hauff, R. Rothe, R. Scholz, U. Gneveckow, P. Wust, B. Thiesen, A. Feussner, A. von Deimling, N. Waldoefner, R. Felix and A. Jordan, *J Neurooncol*, 2007, **81**, 53-60.
7. C. H. Choi, J. E. Zuckerman, P. Webster and M. E. Davis, *Proc Natl Acad Sci U S A*, 2011, **108**, 6656-6661.
8. Q. Dai, C. Walkey and W. C. Chan, *Angew Chem Int Ed Engl*, 2014, **53**, 5093-5096.
9. F. Sonvico, S. Mornet, S. Vasseur, C. Dubernet, D. Jaillard, J. Degrouard, J. Hoebeke, E. Duguet, P. Colombo and P. Couvreur, *Bioconjugate Chem*, 2005, **16**, 1181-1188.
10. J. Xie, K. Chen, H. Y. Lee, C. Xu, A. R. Hsu, S. Peng, X. Chen and S. Sun, *J Am Chem Soc*, 2008, **130**, 7542-7543.
11. C. G. Hadjipanayis, R. Machaidze, M. Kaluzova, L. Wang, A. J. Schuette, H. Chen, X. Wu and H. Mao, *Cancer Res*, 2010, **70**, 6303-6312.
12. F. Li, L. Zhang and R. M. Metzger, *Chemistry of Materials*, 1998, **10**, 2470-2480.
13. H. Maeda, J. Wu, T. Sawa, Y. Matsumura and K. Hori, *J Control Release*, 2000, **65**, 271-284.
14. Y. Zhang, M. DaSilva, B. Ashall, G. Doyle, D. Zerulla, T. D. Sands and G. U. Lee, *Langmuir*, 2011, **27**, 15292-15298.
15. D. Kilinc, J. M. Peyrin, V. Soubeyre, S. Magnifico, L. Saias, J. L. Viovy and B. Brugg, *Neurotox Res*, 2011, **19**, 149-161.
16. D. Kilinc, A. Blasiak, J. J. O'Mahony, D. M. Suter and G. U. Lee, *Biophys J*, 2012, **103**, 1120-1129.

17. D. L. Huber, *Small*, 2005, **1**, 482-501.
18. J. M. Baik, M. Schierhorn and M. Moskovits, *The Journal of Physical Chemistry C*, 2008, **112**, 2252-2255.
19. R. M. Cornell and U. Schwertmann, *The Iron Oxides: Structure, Properties, Reactions, Occurrences and Uses*, Wiley-VCH Verlag GmbH & Co. KGaA, Weinheim, Germany, 2003.
20. T. Fuchigami, Y. Kitamoto and Y. Namiki, *Biomatter*, 2012, **2**, 313-320.
21. N. Kang, J. H. Park, J. Choi, J. Jin, J. Chun, I. G. Jung, J. Jeong, J. G. Park, S. M. Lee, H. J. Kim and S. U. Son, *Angew Chem Int Ed Engl*, 2012, **51**, 6626-6630.
22. J. W. Tavacoli, P. Bauer, M. Fermigier, D. Bartolo, J. Heuvingh and O. du Roure, *Soft Matter*, 2013, **9**, 9103-9110.
23. R. Fuhrer, C. M. Schumacher, M. Zeltner and W. J. Stark, *Adv Funct Mater*, 2013, **23**, 3845-3849.
24. G. Bowers, D. Reardon, T. Hewitt, P. Dent, R. B. Mikkelsen, K. Valerie, G. Lammering, C. Amir and R. K. Schmidt-Ullrich, *Oncogene*, 2001, **20**, 1388-1397.
25. J. V. Thottassery, Y. Sun, L. Westbrook, S. S. Rentz, M. Manuvakhova, Z. Qu, S. Samuel, R. Upshaw, A. Cunningham and F. G. Kern, *Cancer Res*, 2004, **64**, 4637-4647.
26. Y. Yarden and M. X. Sliwkowski, *Nat Rev Mol Cell Biol*, 2001, **2**, 127-137.
27. M. Hiroshima, Y. Saeki, M. Okada-Hatakeyama and Y. Sako, *Proc Natl Acad Sci U S A*, 2012, **109**, 13984-13989.
28. D. Kilinc and G. U. Lee, *Integr Biol (Camb)*, 2014, **6**, 27-34.
29. C. Bustamante, Y. R. Chemla, N. R. Forde and D. Izhaky, *Annu Rev Biochem*, 2004, **73**, 705-748.
30. G. I. Bell, *Science*, 1978, **200**, 618-627.
31. P. M. Williams, *Analytica Chimica Acta*, 2003, **479**, 107-115.
32. J. Kim, S. Park, J. E. Lee, S. M. Jin, J. H. Lee, I. S. Lee, I. Yang, J. S. Kim, S. K. Kim, M. H. Cho and T. Hyeon, *Angew Chem Int Ed Engl*, 2006, **45**, 7754-7758.
33. L. Wang, J. Bai, Y. Li and Y. Huang, *Angew Chem Int Ed Engl*, 2008, **47**, 2439-2442.
34. C. Xu, J. Xie, D. Ho, C. Wang, N. Kohler, E. G. Walsh, J. R. Morgan, Y. E. Chin and S. Sun, *Angew Chem Int Ed Engl*, 2008, **47**, 173-176.
35. Y. Zhang, B. Ashall, G. Doyle, D. Zerulla and G. U. Lee, *Langmuir*, 2012, **28**, 17101-17107.
36. J. E. Rosen, L. Chan, D. B. Shieh and F. X. Gu, *Nanomed-Nanotechnol*, 2012, **8**, 275-290.
37. C. G. Hadjipanayis, M. J. Bonder, S. Balakrishnan, X. Wang, H. Mao and G. C. Hadjipanayis, *Small*, 2008, **4**, 1925-1929.
38. B. Mehdaoui, A. Meffre, J. Carrey, S. Lachaize, L.-M. Lacroix, M. Gougeon, B. Chaudret and M. Respaud, *Adv Funct Mater*, 2011, **21**, 4573-4581.
39. L. M. Lacroix, N. F. Huls, D. Ho, X. Sun, K. Cheng and S. Sun, *Nano Lett*, 2011, **11**, 1641-1645.